Microbial iron limitation in the ocean's twilight zone

https://doi.org/10.1038/s41586-024-07905-z

Received: 13 December 2023

Accepted: 5 August 2024

Published online: 25 September 2024



Check for updates

Jingxuan Li^{1,2,11}, Lydia Babcock-Adams^{3,11}, Rene M. Boiteau⁴, Matthew R. McIlvin¹, Lauren E. Manck⁵, Matthias Sieber⁶, Nathan T. Lanning^{2,7}, Randelle M. Bundy⁸, Xiaopeng Bian9, Iulia-Mădălina Ştreangă1,2, Benjamin N. Granzow1,10, Matthew J. Church5, Jessica N. Fitzsimmons⁷, Seth G. John⁹, Tim M. Conway⁶ & Daniel J. Repeta^{1⊠}

Primary production in the sunlit surface ocean is regulated by the supply of key nutrients, primarily nitrate, phosphate and iron (Fe), required by phytoplankton to fix carbon dioxide into biomass¹⁻³. Below the surface ocean, remineralization of sinking organic matter rapidly regenerates nutrients, and microbial metabolism in the upper mesopelagic 'twilight zone' (200-500 m) is thought to be limited by the delivery of labile organic carbon^{4,5}. However, few studies have examined the role of nutrients in shaping microbial production in the mesopelagic⁶⁻⁸. Here we report the distribution and uptake of siderophores, biomarkers for microbial Fe deficiency across a meridional section of the eastern Pacific Ocean. Siderophore concentrations are high not only in chronically Fe-limited surface waters but also in the twilight zone underlying the North and South Pacific subtropical gyres, two key ecosystems for the marine carbon cycle. Our findings suggest that bacterial Fe deficiency owing to low Fe availability is probably characteristic of the twilight zone in several large ocean basins, greatly expanding the region of the marine water column in which nutrients limit microbial metabolism, with potential implications for ocean carbon storage.

Nutrients are regenerated from sinking particles at different rates. $Owing \, to \, slow \, remineralization \, and \, intense \, scavenging ^{10,11}, Fe \, increases$ in concentration much more slowly with depth than nitrate or phosphate¹²⁻¹⁴. Fe is critical to a suite of enzymes that catalyse the metabolism of organic matter and culture studies show that the cellular Fe requirements of heterotrophic bacteria are relatively high^{15,16}. The slow increase in dissolved iron (DFe) concentrations with depth together with the high Fe requirements of heterotrophic bacteria raise the potential for Fe limitation of bacterial metabolism in mesopelagic waters. which—in turn—could have consequences for the transfer of carbon from the surface into the deep ocean.

Nearly all DFe in seawater is complexed to ligands that act to both elevate DFe concentrations and affect Fe bioavailability^{17,18}. Most ligands are by-products of organic matter degradation and have low binding affinities for Fe (refs. 19,20). However, as Fe concentrations approach limiting values or as Fe becomes less bioavailable, some bacteria secrete siderophores, low-molecular-weight metabolites synthesized specifically for their high Fe affinity9. Siderophores form strong complexes with DFe and facilitate Fe uptake through specialized transporters that recognize the Fe-siderophore complex. Siderophore production and uptake comes with a steep fitness cost to bacteria inhabiting low-energy environments such as the mesopelagic ocean. Carbon and energy that would otherwise be allocated to biomass production and growth are instead allocated to Fe acquisition. Metabolic models and cultivation experiments show that siderophore biosynthesis and uptake is favourable only when Fe limits growth²¹. Siderophores can therefore serve as biomarkers for microbial Fe stress in situ.

As part of the GEOTRACES GP15 expedition, we measured the distribution of siderophores and DFe across a section of the eastern Pacific Ocean extending from 56° N to 20° S along 152° W (Fig. 1a). The GP15 section traverses several biogeochemical provinces, including Fe-rich productive coastal waters along the south Alaskan Shelf, the chronically Fe-limited subpolar gyre and eastern equatorial upwelling regions and two large oligotrophic subtropical (North and South Pacific) gyres. Overall, the section offered the opportunity to both compare the distribution of siderophores with DFe and identify regions of microbial Fe stress across the different nutrient regimes that characterize the Pacific Ocean.

Fe deficiency in the twilight zone

The most notable feature of the GP15 section was the high concentrations of siderophores in surface waters of the subpolar gyre (stations 4-10; Fig. 1b) and equatorial upwelling areas (stations 25-34), and throughout the upper mesopelagic twilight zone (200-500 m) underlying both the North and South Pacific subtropical gyres (stations 12-23 and 35-39, respectively). Unexpectedly high concentrations (3-12 pM) of siderophores in mesopelagic samples relative to overlying surface

Department of Marine Chemistry and Geochemistry, Woods Hole Oceanographic Institution, Woods Hole, MA, USA. 2Department of Earth, Atmospheric, and Planetary Sciences, Massachusetts Institute of Technology, Cambridge, MA, USA. 3 Ion Cyclotron Resonance Program, National High Magnetic Field Laboratory, Florida State University, Tallahassee, FL, USA. 4Department of Chemistry, University of Minnesota, Minneapolis, MN, USA. ⁵Flathead Lake Biological Station, University of Montana, Polson, MT, USA. ⁶College of Marine Science, University of South Florida, St Petersburg, FL, USA. 7Department of Oceanography, Texas A&M University, College Station, TX, USA. 8School of Oceanography, University of Washington, Seattle, WA, USA. 9Department of Earth Sciences, University of Southern California, Los Angeles, CA, USA. 10Geosciences Research Division, Scripps Institution of Oceanography, La Jolla, CA, USA. 11These authors contributed equally: Jingxuan Li, Lydia Babcock-Adams. [™]e-mail: drepeta@whoi.edu

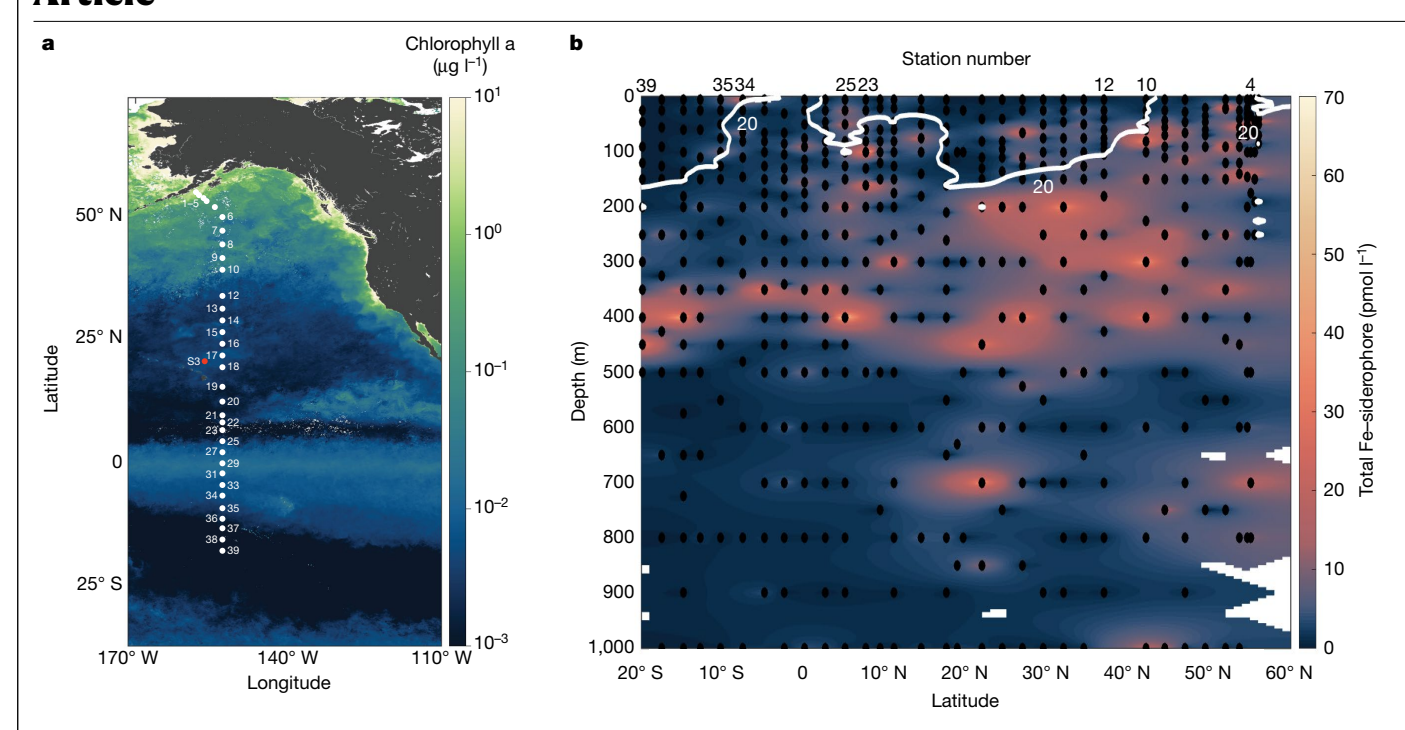


Fig. 1 | High siderophore concentrations in the mesopelagic of the eastern Pacific Ocean. a, Cruise track of the GP15 section showing the locations of sampling stations (1-39) overlaid on Aqua MODIS-derived average sea-surface chlorophyll during the time of the cruise (October–December 2018). Station S3, the location of ⁵⁷Fe-siderophore uptake experiments, is shown in red. **b**, The distribution of total Fe-siderophores in the upper 1,000 m of GP15. Sample locations are denoted by black circles in the plot. Station numbers are at the top

of the plot. Total concentrations of Fe-siderophores were calculated by summing all Fe-siderophores with a concentration > 0.5 pM. The white contour line indicates where the nitrate: DFe ratio transitions from values <20 µmol nmol⁻¹ at depths shallower than the contour to values >20 µmol nmol⁻¹ below it. For stations 1-7, the region with nitrate:DFe ratio <20 µmol nmol⁻¹ lies within the contour.

waters (1-2 pM) have been reported in the past, suggesting that the heterotrophic community at depth may be Fe stressed⁷. In the GP15 samples, concentrations of siderophores in mesopelagic waters reached values of 68 pM, equal to their maximum concentrations (66 pM) in surface waters of the subpolar gyre. For samples in which siderophore concentrations were >1 pM, siderophores accounted for between 0.1 and 80.0% of DFe.

Siderophores are produced in response to low DFe (refs. 22.23), but the siderophore concentration across GP15 did not correlate with DFe. In fact, siderophores were undetectable (<0.5 pM) in many samples with low concentrations of DFe (<100 pM), whereas a few samples with high DFe (>800 pM) also had high concentrations of siderophores (>10 pM; Fig. 2a). The distribution of DFe and siderophores across the eastern Pacific Ocean indicates that DFe concentration alone is not a good indicator for Fe stress of bacteria²⁴ (Fig. 2a).

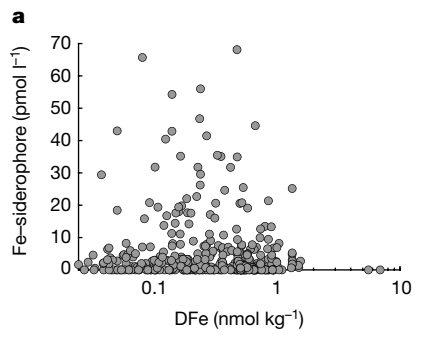
Heterotrophic bacteria collected from the Fe-limited subpolar Pacific Ocean had a cellular N:Fe ratio of 20 μmol nmol⁻¹, similar to bacteria grown in low DFe laboratory cultures, which had maximum cellular N:Fe ratios of 20–500 µmol nmol⁻¹ (refs. 15,16). In chronically Fe-limited surface waters, nutrients are supplied from deeper waters that are relatively enriched in nitrate and depleted in DFe (ref. 14). The supply of Fe to these regions is not sufficient to support the complete drawdown of all available nitrate through biological production, leading to Fe limitation²⁵. When siderophore concentrations across GP15 were plotted against nitrate:DFe ratio, 215 of 262 samples in which siderophores were detected and 28 of 30 samples with high (>20 pM) siderophore concentrations were associated with nitrate:DFe ratios >20 μmol nmol⁻¹ (Fig. 2b).

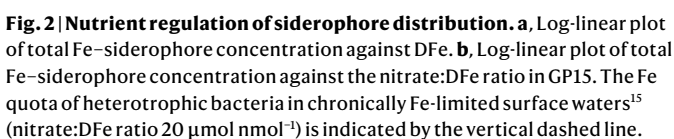
As predicted from the nitrate:DFe ratio, siderophore concentrations were high in the sunlit euphotic zone of the subpolar gyre and equatorial upwelling regions (Fig. 1b). By contrast, surface waters of the North and South Pacific subtropical gyres have an average nitrate:DFe ratio of about 10 μmol nmol⁻¹, and siderophores were only occasionally detected at low concentrations in these samples. However, siderophore concentrations were high in the mesopelagic zone (200–500 m) underlying the North and South Pacific subtropical gyres, which were characterized by nitrate:DFe ratio >20 µmol nmol⁻¹. Deeper in the ocean, below 500 m, as the supply of labile organic carbon from sinking particles decreases, there is presumably a concomitant reduction in microbial Fe demand. Siderophores were occasionally detected at depths >500 m, but only in low concentrations (approximately 2 pM).

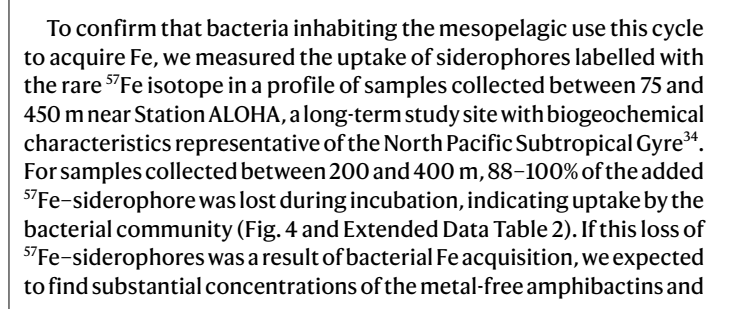
Nearly all siderophores measured across the GP15 section were identified as Fe-amphibactins and Fe-marinobactins^{26,27} (Extended Data Figs. 1 and 2). The amphiphilic character of amphibactins and marinobactins allows them to associate with cell membranes. This association facilitates uptake after Fe binding and mitigates the diffusive loss of the siderophores into the environment^{28,29}. However, we did not detect amphibactins or marinobactins in samples of suspended particulate matter collected concurrently with our water samples, even in mesopelagic samples with high concentrations of dissolved amphibactins and marinobactins (Extended Data Table 1). Although we cannot rule out that siderophore-membrane associations disintegrated during particulate matter collection, our measurements point to siderophores as part of the dissolved ($<0.2 \,\mu m$) fraction of marine Fe.

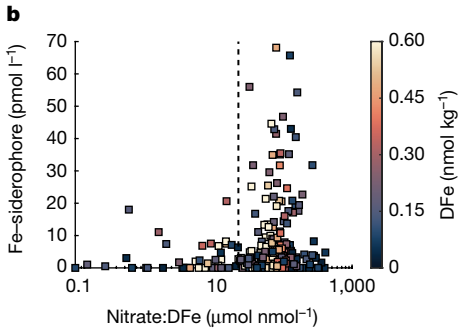
Fe uptake from siderophores

In seawater, siderophores complex Fe from weaker ligands (Fig. 3). The Fe-siderophore complex then binds to siderophore-specific membrane transporters, which deliver the complex into the cell 30,31 , in which Fe is recovered³². The Fe-free siderophore is then returned to the environment to repeat the cycle³³ (Fig. 3).



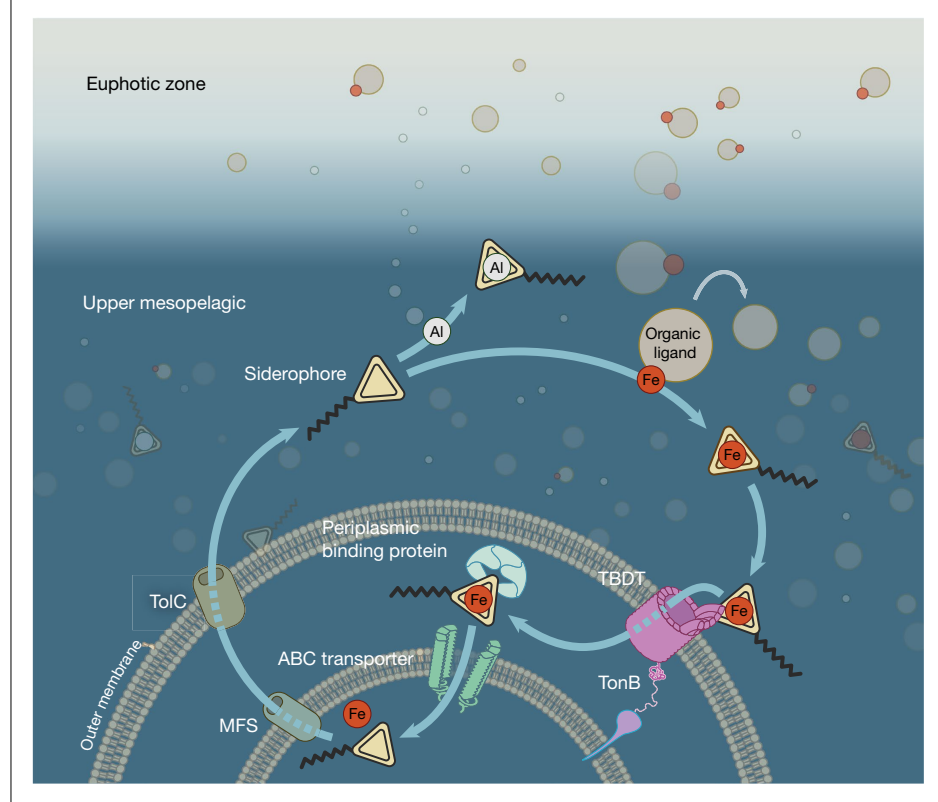






The orders-of-magnitude change in the nitrate: DFe ratio (horizontal axis) is driven by the rapid changes in nitrate concentrations with depth in the mesopelagic. The colour of the symbols in **b** represents concentrations of DFe for each sample.

marinobactins in the samples after incubation, as shown in Fig. 3. However, if the ⁵⁷Fe-amphibactins and ⁵⁷Fe-marinobactins were used as sources of labile carbon and nitrogen, no increase in metal-free siderophores should have occurred. To distinguish these two outcomes and to measure the fraction of uptake allocated to Fe acquisition, inorganic $^{57}\mbox{Fe}$ was added to the sample extracts and the extracts reanalysed. Any metal-free siderophores secreted by bacteria following Fe uptake will complex with the newly added ⁵⁷Fe and be measured as an increase in the concentration of ⁵⁷Fe-siderophores. Addition of ⁵⁷Fe to the mesopelagic samples increased siderophore concentrations to roughly



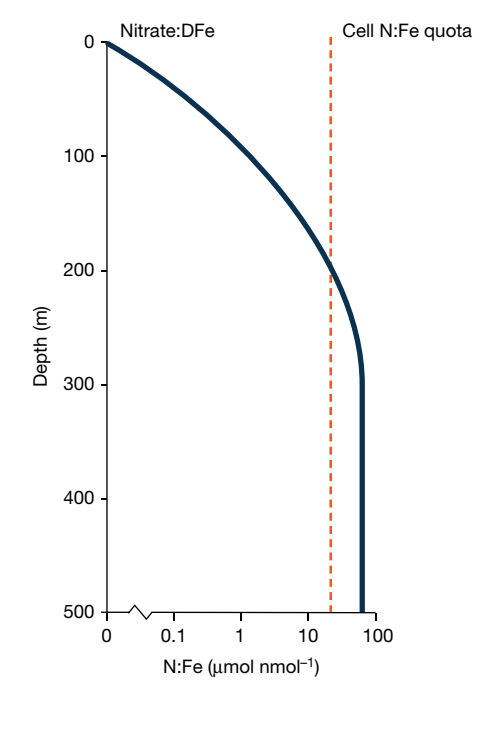
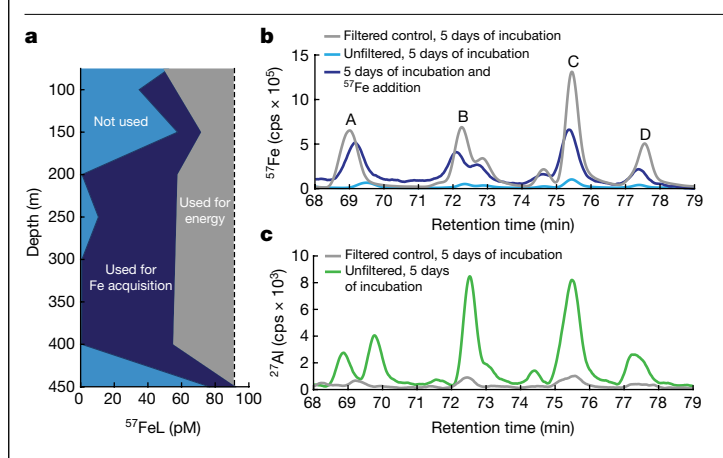


Fig. 3 | Fe-siderophore cycling in the mesopelagic ocean. Marine bacteria acquire Fe and cycle siderophores between the cell and the environment through several different species-dependent pathways 30. In the generalized scheme shown here, metal-free siderophores bind Fe from weaker organic ligands dissolved in seawater and the Fe-siderophore complex is then transported through the outer membrane of gram-negative bacteria by means of TonBdependent transporters (TBDT). Siderophores can also bind aluminium, thereby decreasing the efficiency of the siderophore Fe acquisition pathway.

After passing through the outer membrane, the Fe-siderophore complex $binds \ to \ a periplasmic \ binding \ protein for \ transport \ into \ the \ cytoplasm, in$ which Fe is recovered. Siderophores in the cytoplasm are exported into the environment through major facilitator subtype (MFS) and TolC protein complexes³¹. Siderophore-mediated Fe acquisition is active in the mesopelagic at depths at which the nitrate: DFe ratio $(right)^{45}$ exceeds the maximum N:Fe $quota\,of\,heterotrophic\,bacteria^{15}\,and\,at\,which\,there\,is\,sufficient\,labile\,carbon$ substrate to fuel Fe demand.



 $Fig.\,4\,|\,Cycling\,of sider ophores\,for\,Fe\,in\,the\,twilight\,zone\,of\,the\,North$ Pacific Subtropical Gyre. a, Allocation of siderophores in ⁵⁷Fe-siderophore amendment peak C (shown in panel **b**) with depth after 5 days of incubation. The vertical dashed line indicates the average concentration of siderophore peak C in the filtered control. The light blue shaded region traces the 57 Fesiderophores that remained in the sample at the end of the experiment and the dark blue shaded region is the Fe-siderophores used for Fe acquisition. The grey shaded region shows the siderophore metabolized as labile carbon substrate and not recovered after the incubation. b, Overlay of 57 Fe chromatograms for the filtered control at 200 m after 5 days of incubation, the unfiltered sample at 200 m after 5 days of incubation and the same sample after addition of 57 Fe to the sample extract. The increase in peak concentrations after ⁵⁷Fe addition is because of the complexation of ⁵⁷Fe by Fe-free siderophores in the sample extract. Each peak is a combination of a 57 Fe-amphibactin and a ⁵⁷Fe-marinobactin (Extended Data Fig. 3). **c**, Overlay of ²⁷Al chromatograms for the filtered control and unfiltered sample from 200 m after 5 days of incubation showing the increase in Al-siderophores during incubation owing to the complexation of dissolved aluminium by metal-free siderophores excreted after Fe uptake. cps, counts per second.

63% of the original amendment (Extended Data Table 3). No metal-free siderophores were detected in the 75-m sample. At 150 m, intermediate between the euphotic and mesopelagic twilight zones, 25% of the original amendment was taken up to acquire Fe, whereas at 450 m, 19% of the siderophore amendment was used to acquire Fe. The slower Fe uptake at 450 m compared with 400 m was most probably because of a sharp decrease in Fe demand in response to the attenuation of sinking organic carbon with depth. Between 11 and 37% of the siderophore amendment was not recovered even following the addition of ⁵⁷Fe, indicating that—at all depths—a fraction of the siderophore amendment was metabolized as labile carbon substrate.

Accompanying the loss of the ⁵⁷Fe-siderophores in the mesopelagic samples, we noted increases in the concentrations of ²⁷Al-siderophores (Extended Data Table 2). For example, at 250 m, the total concentration of ⁵⁷Fe-marinobactin C and ⁵⁷Fe-amphibactin T (Fig. 4 peak C) decreased by 81 pM (89%), whereas-concurrently-the concentration of ²⁷Al-peak C increased by 3.4 pM (Extended Data Table 2). Siderophores are known to complex with Al (ref. 35) and suites of Al-marinobactins and Al-amphibactins were found alongside their Fe homologues across the GP15 section. The increase in Al-siderophore concentrations during the incubation experiment provides further evidence that bacteria acquired Fe from amphibactins and marinobactins and secreted the metal-free siderophores back into the environment (Fig. 3).

The zone of Fe-siderophore uptake in the ⁵⁷Fe experiment aligns with the region of the North and South Pacific mesopelagic with high siderophore concentrations and high nitrate:DFe ratios, confirming that the microbial communities inhabiting these regions experience Fe stress and use siderophores to acquire Fe. The absence of siderophore-mediated Fe uptake in the euphotic zone aligns with the low siderophore and low nitrate: DFe region of the GP15 upper water column. Microbes inhabiting this region use other uptake pathways to acquire Fe and are probably Fe-replete. Between the Fe-replete euphotic zone and the Fe-deficient twilight zone, there is a transition zone characterized by slow uptake of Fe-siderophores, indicating some Fe deficiency.

Mesopelagic Fe cycling in the global ocean

Siderophores are molecular indicators of Fe stress only for the microbes that produce them. Our inference that siderophores provide a broader measure of community Fe stress assumes similar Fe requirements among diverse groups of heterotrophic bacteria, which can only be verified by future studies designed to couple whole community 'omics' data with siderophore production and uptake rate measurements. Nevertheless, Fe bioavailability probably shapes microbial metabolism in the mesopelagic across much of the global ocean. Using the nitrate:DFe ratio >20 μmol nmol⁻¹ as a proxy for bacterial siderophore Fe acquisition, the 200-500-m twilight zones of the South Pacific and Southern oceans (nitrate:DFe $89 \pm 36 \,\mu\text{mol} \,\text{nmol}^{-1}$), Tropical Pacific (nitrate:DFe $79 \pm 45 \,\mu\text{mol nmol}^{-1}$), Arctic (nitrate:DFe $32 \pm 9 \,\mu\text{mol nmol}^{-1}$), Indian (nitrate:DFe 54 ± 46 μmol nmol⁻¹) and the South Atlantic (nitrate:DFe $45 \pm 19 \,\mu\text{mol nmol}^{-1}$) oceans could all be Fe-deficient even when microbial communities in the euphotic zone do not necessarily experience Fe limitation (Extended Data Figs. 4-6). By contrast, Fe stress of heterotrophic bacteria in the mesopelagic North Atlantic Ocean may be restricted to only certain geographic regions of this basin (Extended Data Figs. 4-6).

Below the euphotic zone, the downward flux of labile organic matter acts as the primary control on microbial metabolism, thereby affecting the depths at which microbial Fe deficiency will occur. Most organic matter sinking below the euphotic zone is respired by heterotrophic bacteria^{36,37}, which are a key lever on the ocean's biological carbon pump, the process by which carbon is transported as either dissolved or particulate matter from surface waters into the deep ocean. Fe can affect the export flux of carbon in at least two ways. First, field and laboratory culture experiments show that Fe deficiency substantially decreases bacterial growth rates^{15,38-40}. Slower uptake of organic carbon substrates could lead to higher steady-state concentrations and greater persistence of mesopelagic dissolved organic carbon, a notable reservoir of marine carbon. Second, although bacteria can restructure their metabolism to mitigate Fe deficiency^{16,41}, field and laboratory experiments show that Fe deficiency substantially decreases bacteria growth efficiency^{15,42,43}, the ratio of carbon allocated to biomass production relative to the total carbon consumed to support metabolism. If these studies are representative of the environment, a decrease in bacterial growth efficiency would increase the amount of organic matter respired to carbon dioxide relative to biomass production and attenuate the strength of the biological carbon pump below 500 m (ref. 44). These two competing effects of Fe on heterotrophic metabolism could have different impacts on carbon storage in the

The factors that regulate the ocean's biological carbon pump are still not well understood, but siderophore Fe cycling along with high spectral counts of outer membrane proteins characteristic of Fesiderophore transporters found across large expanses of the mesopelagic Pacific Ocean⁸ and a recent report that labile Fe amendments can increase bacterial production in mesopelagic samples⁶ all suggest that Fe may be an overlooked factor in shaping carbon flux through the ocean's twilight zone. At the global scale, mesopelagic Fe deficiency greatly expands our view of where oceanic microbial production is influenced by this essential trace metal^{2,3}. Future investigations of Fe fertilization as a means to enhance ocean carbon storage therefore need to consider the consequences of mesopelagic nutrient limitation on carbon export into the deep ocean.

Online content

Any methods, additional references, Nature Portfolio reporting summaries, source data, extended data, supplementary information, acknowledgements, peer review information; details of author contributions and competing interests; and statements of data and code availability are available at https://doi.org/10.1038/s41586-024-07905-z.

- Arrigo, K. R. Marine microorganisms and global nutrient cycles. Nature 437, 349-355
- 2. Moore, C. M. et al. Processes and patterns of oceanic nutrient limitation. Nat. Geosci. 6,
- Browning, T. J. & Moore, C. M. Global analysis of ocean phytoplankton nutrient limitation reveals high prevalence of co-limitation. Nat. Commun. 14, 5014 (2023).
- Buesseler, K. O. et al. Metrics that matter for assessing the ocean biological carbon pump. Proc. Natl Acad. Sci. USA 117, 9679-9687 (2020).
- Buesseler, K. O. et al. Revisiting carbon flux through the ocean's twilight zone. Science 5. 316, 567-570 (2007).
- 6. Baltar, F. et al. Specific effects of trace metals on marine heterotrophic microbial activity and diversity: key role of iron and zinc and hydrocarbon-degrading bacteria. Front Microbiol 9 03190 (2018)
- Bundy, R. M. et al. Distinct siderophores contribute to iron cycling in the mesopelagic at station ALOHA Front Mar Sci 5 61 (2018)
- Mazzotta, M. G., McIlvin, M. R. & Saito, M. A. Characterization of the Fe metalloproteome of a ubiquitous marine heterotroph, Pseudoalteromonas (BB2-AT2): multiple bacterioferritin copies enable significant Fe storage. Metallomics 12, 654-667 (2020).
- 9. Bagg, A. & Neilands, J. B. Molecular mechanism of regulation of siderophore-mediated iron assimilation. Microbiol. Rev. 51, 509-518 (1987).
- Bressac, M. et al. Resupply of mesopelagic dissolved iron controlled by particulate iron composition. Nat. Geosci. 12, 995-1000 (2019).
- Twining, B. S. et al. Differential remineralization of major and trace elements in sinking diatoms. Limnol. Oceanogr. 59, 689-704 (2014).
- Bruland, K. W., Orians, K. J. & Cowen, J. P. Reactive trace metals in the stratified central North Pacific. Geochim. Cosmochim. Acta 58, 3171-3182 (1994).
- Boyd, P. W., Ellwood, M. J., Tagliabue, A. & Twining, B. S. Biotic and abiotic retention, recycling and remineralization of metals in the ocean, Nat. Geosci, 10, 167-173 (2017)
- Schlitzer, R. et al. The GEOTRACES Intermediate Data Product 2017. Chem. Geol. 493,
- Tortell, P. D., Maldonado, M. T. & Price, N. M. The role of heterotrophic bacteria in iron-limited ocean ecosystems. Nature 383, 330-332 (1996).
- Fourquez, M. et al. Effects of iron limitation on growth and carbon metabolism in oceanic and coastal heterotrophic bacteria, Limnol, Oceanogr, 59, 349-360 (2014).
- van den Berg, C. M. Evidence for organic complexation of iron in seawater. Mar. Chem. 50, 139-157 (1995)
- Rue, E. L. & Bruland, K. W. Complexation of iron(III) by natural organic ligands in the Central North Pacific as determined by a new competitive ligand equilibration/adsorptive cathodic stripping voltammetric method, Mar. Chem. 50, 117-138 (1995).
- Gledhill, M. & Buck, K. N. The organic complexation of iron in the marine environment: a review. Front. Microbiol. 3, 69 (2012).
- 20. Hassler, C. S., van den Berg, C. M. G. & Boyd, P. W. Toward a regional classification to provide a more inclusive examination of the ocean biogeochemistry of iron-binding ligands. Front. Mar. Sci. 4, 19 (2017).
- Sexton, D. J. & Schuster, M. Nutrient limitation determines the fitness of cheaters in bacterial siderophore cooperation. Nat. Commun. 8, 230 (2017).
- Sijerčić, A. & Price, N. M. Hydroxamate siderophore secretion by Pseudoalteromonas haloplanktis during steady-state and transient growth under iron limitation. Mar. Ecol. Prog. Ser. 531, 105-120 (2015).
- Gauglitz, J. M. et al. Dynamic proteome response of a marine Vibrio to a gradient of iron and ferrioxamine bioavailability. Mar. Chem. 229, 103913 (2021).

- Park, J. et al. Siderophore production and utilization by marine bacteria in the North Pacific Ocean. Limnol. Oceanogr. 68, 1636-1653 (2023)
- Martin, J. H. et al. Testing the iron hypothesis in ecosystems of the equatorial Pacific Ocean. Nature 371, 123-129 (1994).
- Martinez, J. S. et al. Structure and membrane affinity of a suite of amphiphilic siderophores produced by a marine bacterium. Proc. Natl Acad. Sci. USA 100, 3754-3759 (2003).
- Martinez, J. S. et al. Self-assembling amphiphilic siderophores from marine bacteria Science 287, 1245-1247 (2000).
- Xu, G., Martinez, J. S., Groves, J. T. & Butler, A. Membrane affinity of the amphiphilic marinobactin siderophores. J. Am. Chem. Soc. 124, 13408-13415 (2002).
- Kramer, J., Özkaya, Ö. & Kümmerli, R. Bacterial siderophores in community and host interactions. Nat. Rev. Microbiol. 18, 152-163 (2020).
- Saha, R., Saha, N., Donofrio, R. S. & Bestervelt, L. L. Microbial siderophores: a mini review. J. Basic Microbiol. 53, 303-317 (2012).
- Wilson, B. R., Bogdan, A. R., Miyazawa, M., Hashimoto, K. & Tsuji, Y. Siderophores in iron metabolism: from mechanism to therapy potential. Trends Mol. Med. 22, 1077-1090 (2016)
- Schalk, I. J. & Guillon, L. Fate of ferrisiderophores after import across bacterial outer membranes: different iron release strategies are observed in the cytoplasm or periplasm depending on the siderophore pathways. Amino Acids 44, 1267-1277 (2013).
- Greenwald, J. et al. Real time fluorescent resonance energy transfer visualization of ferric pyoverdine uptake in Pseudomonas aeruginosa: a role for ferrous iron. J. Biol. Chem. 282, 2987-2995 (2007)
- Karl, D. M. & Church, M. J. Microbial oceanography and the Hawaii Ocean Time-series programme. Nat. Rev. Microbiol. 12, 699-713 (2014).
- Hu, X. & Boyer, G. L. Siderophore-mediated aluminum uptake by Bacillus megaterium ATCC 19213. Appl. Environ. Microbiol. 62, 4044-4048 (1996).
- Giering, S. L. C. et al. Reconciliation of the carbon budget in the ocean's twilight zone. Nature 507, 480-483 (2014).
- Steinberg, D. K. et al. Bacterial vs. zooplankton control of sinking particle flux in the ocean's twilight zone. Limnol. Oceanogr. 53, 1327-1338 (2008).
- Pakulski, J. D. et al. Iron stimulation of Antarctic bacteria. Nature 383, 133-134 (1996).
- Granger, J. & Price, N. M. The importance of siderophores in iron nutrition of heterotrophic marine bacteria. Limnol. Oceanogr. 44, 541-555 (1999).
- Church, M. J., Hutchins, D. A. & Ducklow, H. W. Limitation of bacterial growth by dissolved organic matter and iron in the Southern Ocean. Appl. Environ. Microbiol. 66, 455-466
- Mendonca, C. M. et al. Hierarchical routing in carbon metabolism favors iron-scavenging strategy in iron-deficient soil Pseudomonas species. Proc. Natl Acad. Sci. USA 117, 32358-32369 (2020).
- 42. Kirchman, D. L., Hoffman, K. A., Weaver, R. & Hutchins, D. A. Regulation of growth and energetics of a marine bacterium by nitrogen source and iron availability. Mar. Ecol. Prog. Ser. 250, 291-296 (2003).
- Beier, S. et al. The transcriptional regulation of the glyoxylate cycle in SAR11 in response to iron fertilization in the Southern Ocean. Environ. Microbiol. Rep. 7, 427-434 (2015)
- Kwon, E. Y., Primeau, F. & Sarmeento, J. L. The impact of remineralization depth on the air-sea carbon balance. Nat. Geosci. 2, 630-635 (2009).
- Fitzsimmons, J. N. et al. Daily to decadal variability of size-fractionated iron and iron-binding ligands at the Hawaii Ocean Time-series Station ALOHA, Geochim, Cosmochim. Acta 171, 303-324 (2015).

Publisher's note Springer Nature remains neutral with regard to jurisdictional claims in published maps and institutional affiliations.

Springer Nature or its licensor (e.g. a society or other partner) holds exclusive rights to this article under a publishing agreement with the author(s) or other rightsholder(s); author self-archiving of the accepted manuscript version of this article is solely governed by the terms of such publishing agreement and applicable law.

© The Author(s), under exclusive licence to Springer Nature Limited 2024

Methods

Sample collection and preparation

Seawater samples were collected on the US GEOTRACES cruise GP15, Pacific Meridional Transect (R/V Revelle, RR1814 and RR1815) from 18 September to 24 November 2018. Aqua MODIS level 3 seasonal (21 September to 20 December 2018) chlorophyll concentration products were downloaded at about 4-km spatial resolution as standard mapped images from the NASA Ocean Color website (https://oceancolor.gsfc. nasa.gov).

Each water sample was filtered directly from the trace-metal-clean GTC rosette/GO-FLO bottle sampler through a 0.2-µm Pall AcroPak 200 Supor cartridge into a trace-metal-grade acid-cleaned 4-l polycarbonate bottle for siderophore analysis or an acid-cleaned 2-l or 4-l Nalgene LDPE bottle for dissolved Fe analysis. Samples for siderophores were pumped at 20 ml min $^{-1}$ through Bond Elut ENV solid-phase extraction (SPE) columns (1 g, 6 ml, P/N12255012, Agilent Technologies) that had been previously activated by passing 6 ml each of distilled methanol (MeOH, Optima LC/MS Grade, Fisher Scientific) and ultrapure water (qH $_2$ O, 18.2 M Ω) through the column. SPE columns were frozen (–20 °C) immediately after sample collection and returned to the laboratory for processing. Filtered water samples for dissolved Fe concentration analysis were acidified to pH about 2 with the addition of the equivalent of 1 ml of 12 N Teflon-distilled HCl back on shore and left for at least six months before processing 46 .

Dissolved Fe processing and analysis

Dissolved Fe concentrations were measured in GP15 samples by means of a Neptune multicollector inductively coupled plasma mass spectrometry (ICP-MS) in the Tampa Bay Plasma Facility at the University of South Florida using the isotope dilution technique, following the methods in refs. 46,47. Briefly, acidified seawater samples were amended with a $^{57}\text{Fe}^{-58}\text{Fe}$ double spike solution and 1 ml of 10 mM H_2O_2 , buffered to pH about 6 with ammonium acetate. Dissolved Fe was extracted and purified by means of Nobias PA-1 and AGMP-1 chelating resins before being analysed by ICP-MS. The procedural blank is equivalent to 2 pmol kg $^{-1}$ in a 4-1 sample 47 . The precision and accuracy of this method for dissolved concentrations has been demonstrated previously 46,48,49 , and we express uncertainty (1 s.d.) on Fe concentrations as 2%, based on full replicate analysis of separate GP15 seawater samples collected at the same depth from different bottles (n=26).

Siderophore processing

SPE columns were thawed and washed with 6 ml qH_2O (to reduce salts) and the qH_2O wash was discarded. Ligands were then eluted with 6 ml distilled MeOH into acid-cleaned 10-ml polypropylene tubes. Process blanks were prepared in parallel by eluting activated SPE columns with 6 ml qH_2O followed by 6 ml MeOH. The methanol fraction was collected as the process blank. For consistency among samples, the qH_2O wash and MeOH extraction were performed by a trace-metal-clean liquid handler (model GX-271, Gilson).

A 10-µl stock solution of 2.2 µM Ga-desferrioxamine E (Ga-DFOE) was added to each sample as an internal standard. The sample was concentrated to approximately 500 µl by vacuum centrifugation (SpeedVac, Thermo Scientific; 35 °C, 5 h). A 100-µl aliquot of the sample was taken, mixed with 100 µl of qH₂O and immediately analysed by liquid chromatography–mass spectrometry (LC-MS).

To prepare the Ga-DFOE internal standard, 0.5 mg desferrioxamine E (DFOE; Biophore Research) was dissolved with sonication in 1 ml distilled MeOH. Then, 10 μ l of 200 mM gallium nitrate in qH $_2$ O adjusted to pH 1 with nitric acid (Optima grade, Fisher Scientific) was added to complex DFOE. The solution was diluted with 4 ml qH $_2$ O to make 5 ml of standard. To remove excess Ga, 500 μ l of the solution was applied to a SPE column (C18; 100 mg, 1 ml, Agilent Technologies), which had been previously activated with 2 ml each of distilled MeOH and qH $_2$ O.

The column was washed with 2 ml qH_2O to remove excess Ga and the Ga-DFOE eluted with 2 ml MeOH. The MeOH eluant was collected and then diluted with qH_2O to a final volume of 20 ml.

Quantitative analyses of siderophores

Chromatographic analyses were performed on a bioinert Dionex Ulti-Mate 3000 HPLC system fitted with a loading pump, a nano pump and a ten-port switching valve⁵⁰. During the loading phase, 200 µl of sample were withdrawn into the sample loop, then applied to a C18 trap column $(3.5 \,\mu\text{m}, 0.5 \,\text{mm} \times 35 \,\text{mm}, P/N \,5064 - 8260, Agilent Technologies)$ by the loading pump at 25 µl min⁻¹ for 10 min. The loading solvent is a mixture of 95% solvent A (5 mM aqueous ammonium formate, Optima, Fisher Scientific) and 5% solvent B (5 mM methanolic ammonium formate). During the elution phase, the solvent was delivered by a nano pump at 10 μl min⁻¹ and the trap column outflow directed onto two C18 columns $(3.5 \,\mu\text{m}, 0.5 \,\text{mm} \times 150 \,\text{mm}, P/N \,5064 - 8262, Agilent Technologies) con$ nected in series. Samples were separated with an 80-min linear gradient from 95% solvent A and 5% solvent B to 95% solvent B, followed by isocratic elution at 95% solvent B for 10 min. Meanwhile, the loading pump solvent was switched to 100% qH₂O, the flow rate increased to 35 μl min⁻¹ and directed as a post-column make-up flow, which was infused with the column eluant into the inductively coupled plasma mass spectrometer⁵⁰. The high aqueous content of the combined flow serves to minimize the effect of changes in solvent composition (in this case, increasing methanol content during the analysis) on the detector response to Fe, Ga and Al (ref. 51). For station 39, the HPLC eluant at 10 µl min⁻¹ was directed into the inductively coupled plasma mass spectrometer without post-column infusion of gH₂O.

The combined flow from the liquid chromatograph ($45 \,\mu l \,min^{-1}$) was analysed using a Thermo Scientific iCAP Q ICP-MS fitted with a perfluoroalkoxy micronebulizer (PFA-ST, Elemental Scientific) and a cyclonic spray chamber cooled to $4\,^{\circ}$ C (ref. 52). Measurements were made in kinetic energy discrimination mode, with a helium collision gas flow of $4.0-4.5 \,ml \,min^{-1}$ to minimize isobaric 40 Ar 16 O $^{+}$ interferences on 56 Fe. Oxygen was introduced into the sample carrier gas at $25 \,ml \,min^{-1}$ to prevent the formation of reduced organic deposits onto the inductively coupled plasma mass spectrometer skimmer and sampling cones. Isotopes monitored were 56 Fe (integration time $0.05 \, s$), 54 Fe ($0.02 \, s$), 57 Fe ($0.02 \, s$), 59 Ga ($0.05 \, s$), 71 Ga ($0.02 \, s$) and 27 Al ($0.02 \, s$).

The Fe detector response was calibrated using the siderophore ferrichrome, which elutes at about 40 min in our chromatographic analysis. Stock solutions of 250 μ M ferrichrome were diluted to prepare standards with 2 nM, 5 nM, 10 nM, 20 nM and 40 nM of the siderophore. Then, 5 μ l of 2.2 μ M Ga-DFOE was added to 995 μ l of each standard, a 100- μ l aliquot was taken, mixed with 100 μ l of qH₂O and analysed by LC-ICP-MS. A plot of the ratio ⁵⁶Fe(ferrichrome): ⁶⁹Ga (Ga-DFOE) peak areas against ferrichrome/Ga-DFOE concentration yields a linear relationship ($r^2 \approx 0.999$) for the response of the ICP-MS detector to Fe between 0.2 and 4.0 pmol of ferrichrome. Calibrations and process blanks were made for every 10–20 samples analysed, with only small changes (relative s.d. \approx 30%) being observed in the slope of the calibration relationship over the course of the two years of sample analysis. Concentrations of Fe ligands in each sample were measured by plotting the FeL/Ga-DFOE peak area on the appropriate calibration curve.

Identification of siderophores

To assign Fe–Ls to known siderophores, select samples were analysed by LC-electrospray ionization mass spectrometry (ESIMS). The eluant from the LC, without qH_2O infusion, was coupled to a Thermo Scientific Orbitrap Fusion mass spectrometer equipped with a heated ESI source. ESI source parameters were set to a capillary voltage of 3,500 V, sheath, auxiliary and sweep gas flow rates of 5, 2 and 0 (arbitrary units), respectively, and ion transfer tube and vaporizer temperatures of 275 °C and 20 °C. MS¹ scans for a $\emph{m/z}$ range of 150–1,900 were collected in high-resolution (450 K) positive ion mode.

The LC-ESIMS data were converted from raw file format to mzXML (MSConvert) 53 , imported to MATLAB and aligned with ICP-MS data using the retention time of Ga-DFOE, which was obtained by monitoring m/z of 667.26 by ESIMS and 69 Ga by ICP-MS. The m/z and intensity from each scan were extracted and ordered by scan number into a scan number/mass (m/z)/intensity matrix, which was interrogated by mass search algorithms 50,52 . The algorithms find pairs of co-eluting peaks with a mass difference of 1.995D ($\Delta D = ^{56}$ Fe $- ^{54}$ Fe) and an intensity ratio of 15.7, the crustal abundance ratio of 56 Fe and 54 Fe. Assignments of Fe ligands as known compounds were made by comparing our measured masses to those in a library of 367 known siderophores in the ChelomEx siderophore database 54 and, in some cases, by comparison with amphibatins and marinobatins isolated from laboratory culture.

Preparation of ⁵⁷Fe-labelled amphibactins and marinobactins

Amphibactins were produced by *Vibrio* 1F53 culture under Fe limitation induced by the addition of desferrioxamine B (ref. 50). One litre of culture was pumped at 20 ml min $^{-1}$ through a 0.2- μ m PES capsule filter (Millipore) and Bond Elut ENV SPE column (1 g, 6 ml, Agilent Technologies) that had been previously activated by passing 6 ml each of distilled methanol (MeOH, Optima LC/MS Grade, Fisher Scientific) and ultrapure water (qH $_2$ O, 18.2 M Ω) through the column. After extraction, the column was washed with 6 ml qH $_2$ O and the qH $_2$ O wash was discarded. Amphibactins were then eluted with 6 ml distilled MeOH into acid-cleaned 10-ml polypropylene tubes. Marinobactins were produced by *Alteromonas* 2E5 and *Pseudoalteromonas* 2E11 culture 55 . For each culture, 25 ml of media was pumped through a 0.2- μ m PES Sterivex filter (MilliporeSigma) and C18 SPE columns (0.5 g, Biotage). The SPE column was rinsed with qH $_2$ O and eluted with 5 ml MeOH. The MeOH extracts were concentrated to about 300 μ l under a stream of nitrogen.

Amphibactins produced by *Vibrio* are dominated by non-metallated (apo) siderophores, owing to Fe limitation induced by the presence of 10 nM desferrioxamine B in the culture media 50 . To prepare isotopically labelled amphibactins, 57 Fe oxide (isotope enrichment >95%, Cambridge Isotope Laboratories) was dissolved in concentrated HCl (Optima, Fisher Scientific) as a stock solution of 33.9 mM 57 Fe (180 μ l HCl per 1 mg 57 Fe $_2$ O $_3$). Five microlitres (5 μ l) of this 57 Fe stock solution was added to a 500- μ l aliquot of the amphibactin containing MeOH extract. After one hour, the mixture is diluted to 0.1% MeOH with the addition of 500 ml of qH $_2$ O. The solution was passed through a Bond Elut ENV column (1 g, 6 ml, Agilent Technologies) at 20 ml min $^{-1}$ to remove excess 57 Fe. The SPE columns were then washed with 6 ml of MQ and eluted with 6 ml of MeOH. The MeOH extract was concentrated to approximately 500 μ l by vacuum centrifugation (SpeedVac, Thermo Scientific) and used as amphibactin stock solution.

Marinobactins produced by *Alteromonas* and *Pseudoalteromonas* were recovered as $^{56}\text{Fe}-\text{siderophores}$, owing to the higher concentration of Fe (125 nM) and the absence of desferrioxamine B in the growth media 55 . To label marinobactins with ^{57}Fe , 100 μ l of ^{57}Fe stock solution was added to 10 ml of qH $_2\text{O}$ to create a ^{57}Fe stock solution of pH about 1, which facilitates the isotope exchange from ^{56}Fe to ^{57}Fe . Then, 500 μ l of MeOH extract of *Alteromonas* and *Pseudoalteromonas* were combined and added to the ^{57}Fe stock solution. After 2 days, the mixture was diluted with 1,000 ml of qH $_2\text{O}$, neutralized with 10 ml 100 mM NaHCO $_3$ and extracted by a Bond Elut ENV column. Excess ^{56}Fe and ^{57}Fe passes through the column with the water wash. Then, the column was washed with qH $_2\text{O}$ and eluted with MeOH. The MeOH extract was concentrated to approximately 500 μ l by vacuum centrifugation and used as marinobactin stock solution.

Validation of ⁵⁷Fe-siderophore stock solution

The integrity of the ⁵⁷Fe-siderophore amendment was established by measuring the chromatographic and isotopic properties of the amphibactin or marinobactin mixture by LC-ICP-MS (Extended Data Fig. 2). Fe chromatograms show that ⁵⁶Fe-siderophore accounted for

5–10% of the ⁵⁷Fe–siderophore concentration. Also, both siderophore stock solutions show no Fe eluting at the solvent front on LC-ICP-MS, confirming that the stock solution does not contain inorganic ⁵⁷Fe or ⁵⁶Fe. The baseline is low for both ⁵⁷Fe and ⁵⁶Fe, suggesting that the concentration of other Fe ligand complexes in the stock solutions is also low. Therefore, the Fe added to the incubation by the amendment was dominated by ⁵⁷Fe–siderophores, with little contamination from other Fe ligands, inorganic Fe or ⁵⁶Fe–siderophores.

When amphibactins and marinobactins were mixed, some siderophores co-eluted under the LC conditions used for this study and several siderophores appear as a single peak on ICP-MS. For example, peak A on the chromatogram of amphibactin stock solution (amphibactin $C_{10:1}$) and peak A on the chromatogram of marinobactin (marinobactin A) stock solution co-eluted (Extended Data Fig. 3). Using our chromatographic conditions, ten different peaks were resolved in the 57 Fe chromatogram of the amphibactin/marinobactin amendment, representing more than 20 different siderophores. Each peak includes an Fe–amphibactin and an Fe–marinobactin. All ten peaks were quantified before and after the incubation, but the discussion in the text focuses only on the four main peaks as representative of all siderophores in the mixture. The letters A–D were used to identify the four main peaks, representing 75% of the total siderophores in the amendment.

Peak A is a combination of 57 Fe-amphibactin $C_{10:0}$, and 57 Fe-marinobactin A. Amphibactin $C_{10:0}$ is a new amphibactin that has not been previously reported in the literature. Amphibactin $C_{10:0}$ differs from amphibactin T by $-C_2H_4-$ on the fatty acid chain. Peak B is a combination of 57 Fe-amphibactin $C_{12:1}$ and 57 Fe-marinobactin B. Amphibactin C $_{12:1}$ is also a new amphibactin that differs from amphibactin T by a double bond. Peak C is a combination of 57 Fe-amphibactin T and 57 Fe-marinobactin C. Peak D is a combination of 57 Fe-amphibactin S and 57 Fe-marinobactin D. These siderophores were identified by comparing their exact masses to those in the ChelomEx siderophore database.

To confirm our identifications, high-energy collision-induced dissociation MS² spectra for ⁵⁷Fe-marinobactins and collision-induced dissociation MS² spectra for ⁵⁷Fe-amphibactins were collected on the Orbitrap mass analyser. Ions were trapped using a quadrupole isolation window of 1.6 m/z and were then fragmented using a high-energy collision-induced dissociation collision energy of 30% or collision-induced dissociation collision energy of 35%. The MS² of ⁵⁷Fe-amphibactin T (m/z = 858.384; Extended Data Fig. 3) has major fragments of m/z 486.12.581.26 and 668.29. The fragment at m/z 486.12 represents the cleavage of a peptidic bond on the head group, while retaining ⁵⁷Fe. The fragments at m/z 581.26 and 668.29 represent the cleavage of another two peptidic bonds on the head group that do not retain 57 Fe. These fragmentation patterns are characteristic of amphibactins^{56,57}. The MS² fragmentation spectrum of ⁵⁷Fe-marinobactin C(m/z = 1,014.437) shows major fragments at m/z 486.12, 573.15 and 743.22. For 57 Fe-marinobactin C, the fragment at m/z 486.12 represents diagnostic cleavage of a peptide bond⁵⁸ and a further loss of $H_2O(m/z 18)$. The fragment at m/z 486.12 was also found in the MS² of ⁵⁷Fe-amphibactin T, owing to the same structure of Fe-marinobactin Cand Fe-amphibactin T (N⁵-acyl N⁵-hydroxy ornithine, serine, N⁵-acyl N⁵-hydroxy ornithine) after the neutral loss. Similarly, the fragment at m/z 573.15 represents a diagnostic cleavage of an ornithine-serine peptidic bond and a further loss of H₂O.

Incubation experiments with 57Fe-labelled siderophores

Samples for Fe uptake experiments were collected aboard the R/V Kilo Moana at 23.29° N, 155.32° W near Station ALOHA (22.45° N, 158.0° W) during the SCOPE-PARAGON II expedition in August 2022. Seawater was collected using a Niskin bottle rosette equipped with a conductivity, temperature and depth package (SBE 911plus, Sea-Bird Scientific), along with fluorescence, oxygen and transmissometer sensors. Two litres (2 l) of unfiltered seawater were sampled from nine depths between 75 and 450 m into acid-cleaned 2-l polycarbonate bottles.

Further samples of filtered and unfiltered seawater were taken at 200 and 400 m for experimental controls and measurements of the initial conditions. For the filtered control, samples were filtered directly from the Niskin bottle through an in-line 0.2- μ m AcroPak 1500 Supor cartridge (Pall).

For each incubation sample, 20 μ l of amphibactin stock solution and 20 μ l of marinobactin stock solution were added. The bottles were wrapped in 4-mil black plastic and placed in a temperature-controlled water bath incubator at 25 °C. After 5 days, the samples were filtered and extracted onto SPE columns, frozen immediately (–20 °C) and returned to the laboratory for processing.

Data availability

Siderophore concentration data for the GP15 transect are publicly available through the BCODMO data archive (https://www.bco-dmo.org/dataset/875210 and https://www.bco-dmo.org/dataset/929884). Dissolved iron data for the GP15 transect have been deposited in BCODMO (https://www.bco-dmo.org/dataset/883862 and https://www.bco-dmo.org/dataset/883862 and https://www.bco-dmo.org/dataset/884673). Nitrate data have been deposited in BCODMO (https://www.bco-dmo.org/dataset/777951 and https://www.bco-dmo.org/dataset/824867). The nitrate data in Fig. 3 are from the Hawaii Ocean Time-series (HOT) data archive at the University of Hawaii'i at Manoa (https://hahana.soest.hawaii.edu/hot/methods/llnuts.html). Siderophore concentration data for the uptake experiment are provided at https://zenodo.org/records/12206828. The LC-ESIMS data for Extended Data Figs. 2 and 3 and Extended Data Table 1 are available at MassIVE (https://massive.ucsd.edu/ProteoSAFe/dataset.jsp?task=7439be618f5949ecb1c2eac35978dba4).

- Conway, T. M., Rosenberg, A. D., Adkins, J. F. & John, S. G. A new method for precise determination of iron, zinc and cadmium stable isotope ratios in seawater by doublespike mass spectrometry. *Anal. Chim. Acta* 793, 44–52 (2013).
- Sieber, M. et al. Isotopic fingerprinting of biogeochemical processes and iron sources in the iron-limited surface Southern Ocean. Earth Planet. Sci. Lett. 567, 116967 (2021).
- Middag, R. et al. Intercomparison of dissolved trace elements at the Bermuda Atlantic Time Series station. Mar. Chem. 177, 476–489 (2015).
- Ellwood, M. J. et al. Distinct iron cycling in a Southern Ocean eddy. Nat. Commun. 11, 825 (2020).
- Li, J. et al. Element-selective targeting of nutrient metabolites in environmental samples by inductively coupled plasma mass spectrometry and electrospray ionization mass spectrometry. Front. Mar. Sci. 8, 630494 (2021).
- Boiteau, R. M., Fitzsimmons, J. N., Repeta, D. J. & Boyle, E. A. Detection of iron ligands in seawater and marine cyanobacteria cultures by high-performance liquid chromatographyinductively coupled plasma-mass spectrometry. *Anal. Chem.* 85, 4357-4362 (2013).

- Boiteau, R. M. & Repeta, D. J. An extended siderophore suite from Synechococcus sp. PCC 7002 revealed by LC-ICPMS-ESIMS. Metallomics 7, 877–884 (2015).
- Chambers, M. C. et al. A cross-platform toolkit for mass spectrometry and proteomics. Nat. Biotechnol. 30, 918–920 (2012).
- Baars, O., Morel, F. M. & Perlman, D. H. ChelomEx: isotope-assisted discovery of metal chelates in complex media using high-resolution LC-MS. Anal. Chem. 86, 11298–11305 (2014)
- Boiteau, R. M. Molecular Determination of Marine Iron Ligands by Mass Spectrometry. Thesis, Massachusetts Institute of Technology/Woods Hole Oceanographic Institution (2016).
- Vraspir, J. M., Holt, P. D. & Butler, A. Identification of new members within suites of amphiphilic marine siderophores. *BioMetals* 24, 85–92 (2011).
- Boiteau, R. M. et al. Siderophore-based microbial adaptations to iron scarcity across the eastern Pacific Ocean. Proc. Natl Acad. Sci. 113, 14237–14242 (2016).
- Kem, M. P. & Butler, A. Acyl peptidic siderophores: structures, biosyntheses and post-assembly modifications. *BioMetals* 28, 445–459 (2015).
- GEOTRACES Intermediate Data Product Group. The GEOTRACES Intermediate Data Product 2021 version 2 (IDP2021v2). NERC EDS British Oceanographic Data Centre NOC https://doi.org/10.5285/ff46f034-f47c-05f9-e053-6c86abc0dc7e (2023).
- Xiang, Y. & Lam, P. J. Size-fractionated compositions of marine suspended particles in the Western Arctic Ocean: lateral and vertical sources. J. Geophys. Res. Oceans 125, e2020JC016144 (2020).

Acknowledgements We thank P. Lam, K. Casciotti, G. Cutter, B. Summers and L. Jensen for their organization, assistance and support of the GP15 expedition. P. Morton provided assistance for the inductively coupled plasma mass spectrometry analyses at Texas A&M University. We also thank T. Burrell, R. Tabata, B. Brenes, D. Karl, A. White, P. Kong and M. Seixas for their support and assistance of the PARAGON 2022 cruise on the R/V Kilo Moana. Funding for this work was provided by National Science Foundation Chemical Oceanography Program (NSF awards OCE-1736280 and OCE-2045223 to D.J.R.; OCE-1737167 to J.N.F.; OCE-1737136 to T.M.C.; and OCE-1736896 to S.G.J.). Support was also provided for the Simons Collaboration on Ocean Processes and Ecology programme (SCOPE awards 721227 to D.J.R. and 721221 to M.J.C.), Simons Foundation Early Career Investigator Awards in Marine Microbial Ecology and Evolution (Life Sciences awards 621513 to R.M.Bo and 618401 to R.M.Bu.) and a Simons Foundation Postdoctoral Fellowship in Marine Ecology (award 729162 to L.E.M.).

Author contributions J.L., L.B.-A. and D.J.R. designed the project. J.L. and L.B.-A. collected and processed the GP15 samples. J.L., L.B.-A. and M.R.M. measured and characterized siderophores in the GP15 and PARAGON 2022 samples. D.J.R., J.N.F., R.M.Bo. and R.M.Bu. developed the liquid chromatography—mass spectrometry methods and data interrogation algorithms and purified marinobactins for the PARAGON 2022 experiments. J.L., L.E.M., I.-M.S., B.N.G. and M.J.C. conducted the siderophore uptake experiments during the PARAGON 2022 cruise. M.S., N.T.L., X.B., T.M.C., J.N.F. and S.G.J. measured dissolved iron in the GP15 samples. J.L. and D.J.R. performed the data analysis and wrote the first draft of the paper. All authors contributed to writing the manuscript

Competing interests The authors declare no competing interests.

Additional information

Supplementary information The online version contains supplementary material available at https://doi.org/10.1038/s41586-024-07905-z.

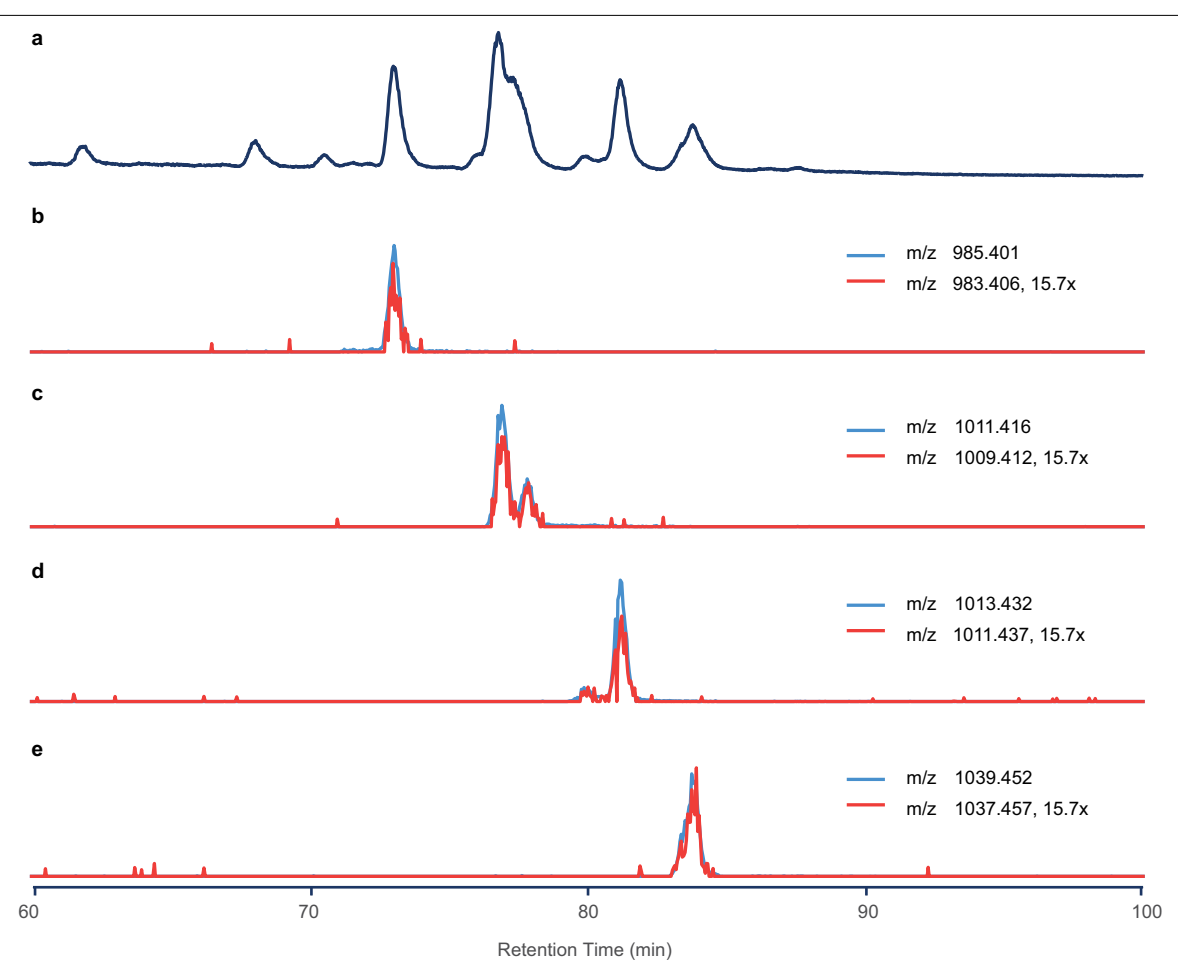
Correspondence and requests for materials should be addressed to Daniel J. Repeta.

Peer review information Nature thanks Martha Gledhill and the other, anonymous, reviewer(s) for their contribution to the peer review of this work. Peer reviewer reports are available.

Reprints and permissions information is available at http://www.nature.com/reprints.

 $\label{lem:extended_DataFig.1} \textbf{Molecular structures of representative marinobactins} \ and \ amphibactins \ identified \ in \ GP15 \ samples. \ Amphibactins \ and \ marinobactins \ are \ distinguished \ by the number \ and \ type \ of \ amino \ acids \ in$

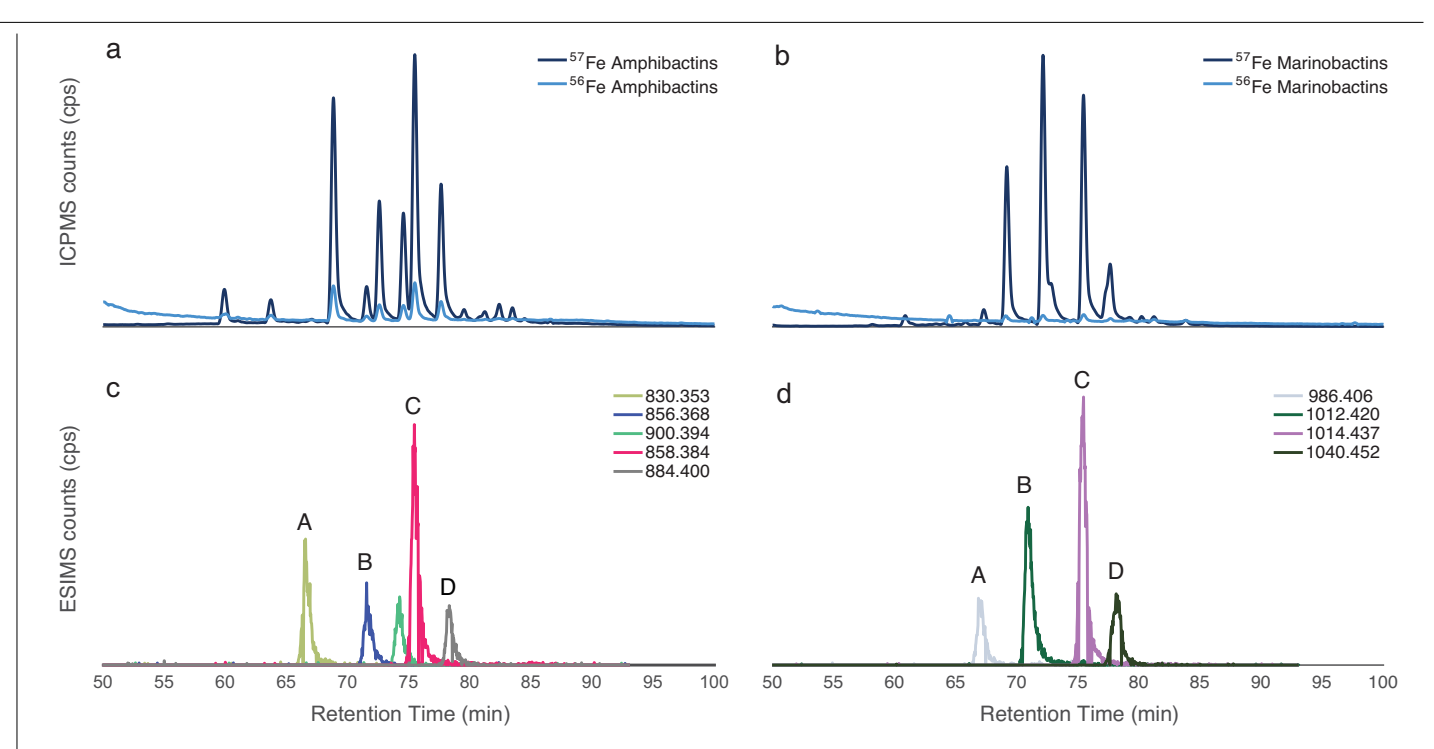
the Fe-complexing peptide head group. Each family of siderophores has several homologues that differ in the number of CH_2 groups and unsaturations in the fatty acid side chain.



$Extended \, Data \, Fig. \, 2 \, | \, Characterization \, of sider ophores \, in \, GP15 \, samples.$

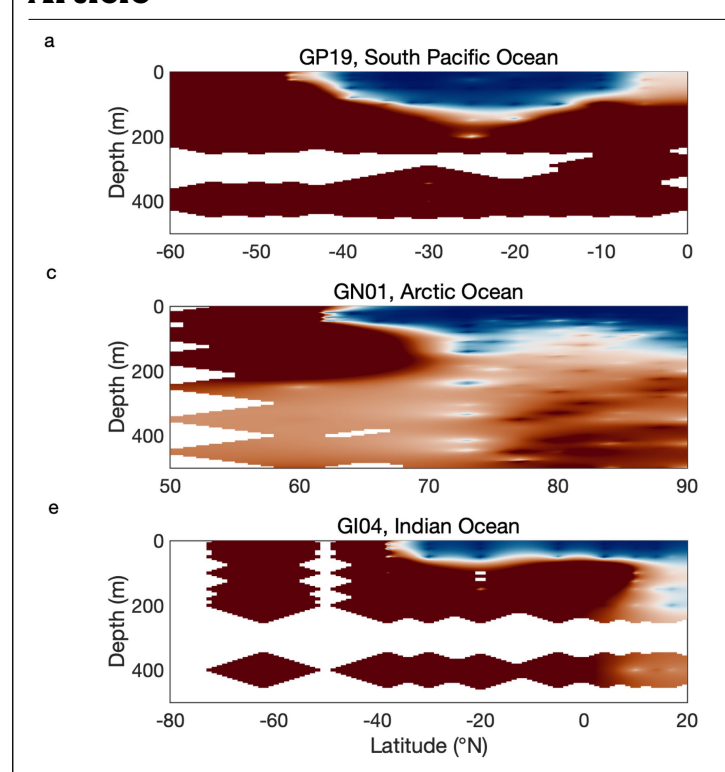
 $\label{eq:continuous} \textbf{a}, The 56Fe chromatogram by LC-ICP-MS for sample at station 16, 400 m. \\ \textbf{b}-\textbf{e}, Extracted ion chromatograms by LC-ESIMS from the same sample. Blue traces correspond to the 56Fe-siderophore [M+H]* isotopologue and red traces correspond to the less abundant 54Fe-siderophore [M+H]* isotopologue.$

The intensity of the 54 Fe isotopologue has been scaled by the 56 Fe/ 54 Fe crustal abundance ratio of 15.7. Peaks were assigned as 56 Fe-marinobactin A (m/z 985.401) (\mathbf{b}), 56 Fe-marinobactin B (m/z1,011.416) (\mathbf{c}), 56 Fe-marinobactin C (m/z1,013.432) (\mathbf{d}) and 56 Fe-marinobactin D (m/z1,039.452) (\mathbf{e}).

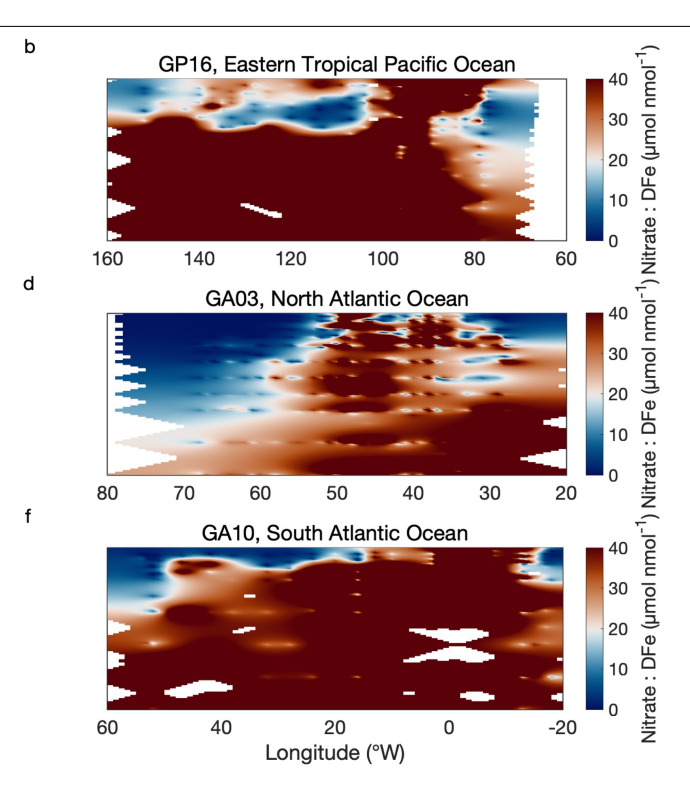


Extended Data Fig. 3 | **Validation of the** 57 Fe-siderophore amendment. 57 Fe (dark blue trace) and 56 Fe (light blue trace) chromatograms of amphibactin (a) and marinobactin (b) mixtures used for the siderophore uptake experiment. c, Extracted ion chromatograms for 57 Fe-amphibactins in the amphibactin stock solution. Peaks were assigned as: A, 57 Fe-amphibactin C $_{10:0}$ (m/z 830.353); B, 57 Fe-amphibactin C $_{12:1}$ (m/z 856.368); C, 57 Fe-amphibactin T (m/z 858.384);

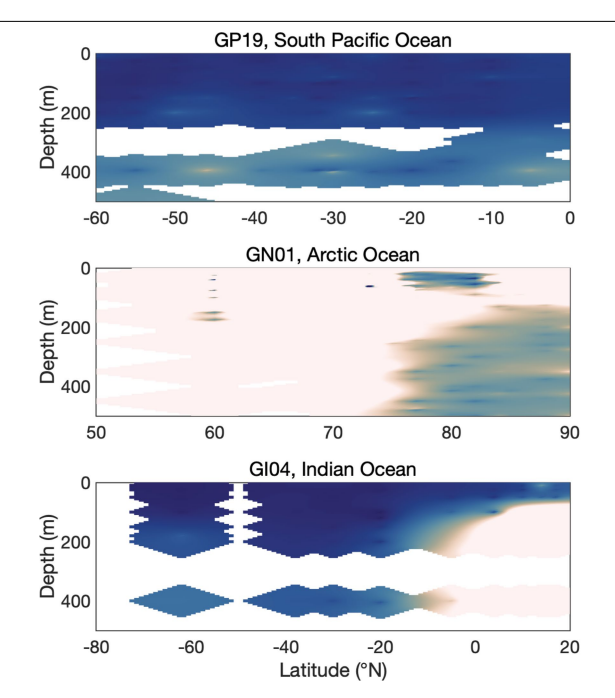
and D, 57 Fe-amphibactin S (m/z 884.400). The peak with an m/z of 900.394 also represents an 57 Fe-amphibactin but does not contribute to the main peaks in Fig. 4. **d**, Extracted ion chromatograms for 57 Fe-marinobactins in the marinobactin stock solution. Peaks were assigned as: A, 57 Fe-marinobactin A (m/z 986.406); B, 57 Fe-marinobactin B (m/z1,012.420); C, 57 Fe-marinobactin C (m/z1,014.437); and D, 57 Fe-marinobactin D (m/z1,040.452).



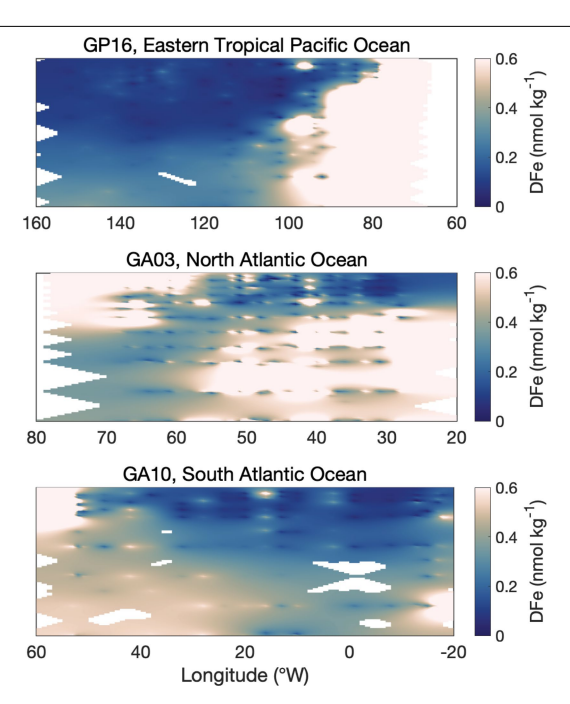
Extended Data Fig. 4 | Sectional plots of nitrate:DFe ratio between the surface and at 500 m in different ocean basins. a, GEOTRACES GP19 section in the South Pacific Ocean along 170° W. b, GEOTRACES GP16 section in the equatorial Pacific Ocean along 10–15° S. c, GEOTRACES GN01 section in the Arctic Ocean along 140° W–180° E. d, GEOTRACES GA03 section in the North



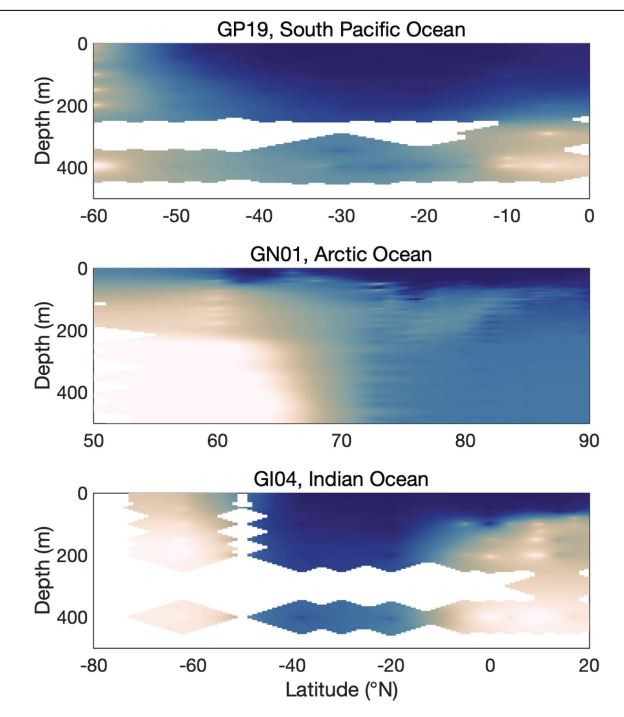
Atlantic Ocean along 15–40° N. e, GEOTRACES GI04 section in the Indian Ocean along 40–85° E. f, GEOTRACES GA10 section in the South Atlantic Ocean along 35–40° S. The data were extracted from GEOTRACES Intermediate Data Product 2017 (ref. 14) and 2021 (ref. 59).



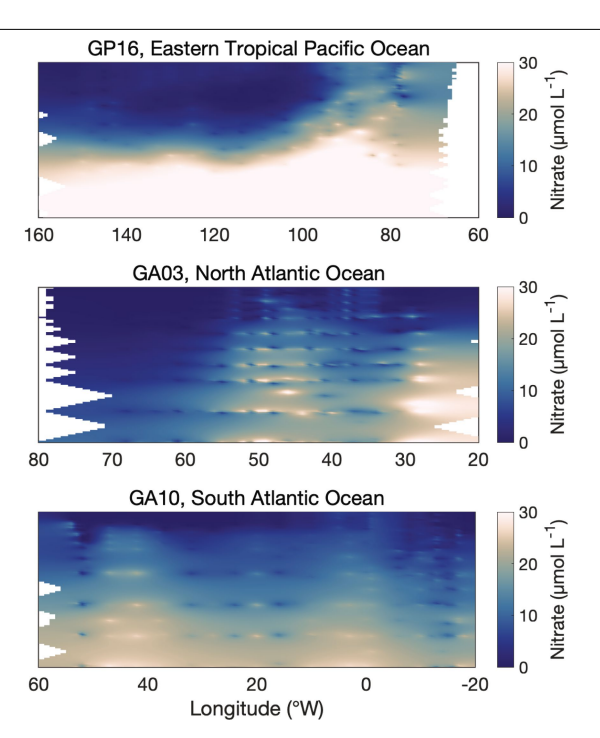
Extended Data Fig. 5 | Sectional plots of DFe concentration between the surface and at 500 m in different ocean basins. a, GEOTRACES GP19 section in the South Pacific Ocean along 170° W. b, GEOTRACES GP16 section in the equatorial Pacific Ocean along 10–15° S. c, GEOTRACES GN01 section in the Arctic Ocean along 140° W–180° E. d, GEOTRACES GA03 section in the North



Atlantic Ocean along 15–40° N. e, GEOTRACES GI04 section in the Indian Ocean along 40–85° E. f, GEOTRACES GA10 section in the South Atlantic Ocean along 35–40° S. The data were extracted from GEOTRACES Intermediate Data Product 2017 (ref. 14) and 2021 (ref. 59).



Extended Data Fig. 6 | Sectional plots of nitrate concentration between the surface and at 500 m in different ocean basins. a, GEOTRACES GP19 section in the South Pacific Ocean along 170° W. b, GEOTRACES GP16 section in the equatorial Pacific Ocean along 10–15° S. c, GEOTRACES GN01 section in the Arctic Ocean along 140° W–180° E. d, GEOTRACES GA03 section in the North



Atlantic Ocean along 15–40° N. e, GEOTRACES GI04 section in the Indian Ocean along 40–85° E. f, GEOTRACES GA10 section in the South Atlantic Ocean along 35–40° S. The data were extracted from GEOTRACES Intermediate Data Product 2017 (ref. 14) and 2021 (ref. 59).

Extended Data Table 1 | The concentration of siderophores in the particulate samples paired with dissolved samples of the closest depth collected at that station

Sample	Station	Depth (m)	[Fe-siderophore]	[Fe-siderophore]	
			Particulate (pM)	Dissolved (pM)	
GT12706	6	38	7.8	66 at 20 m	
GT12707	6	58	2.8	35 at 90 m	
GT12709	6	248	0.04	21 at 250 m	
GT12710	6	348	0.02	21 at 350 m	
GT12875	8	61	0.26	14 at 65 m	
GT12876	8	86	0.04	8 at 90 m	
GT13395	14	71	0.33	5 at 75 m	
GT13396	14	96	0.32	6 at 100 m	
GT13397	14	121	0.16	3 at 125 m	
GT13398	14	145	0.05	11 at 150 m	

The suites of siderophores found in seawater and suspended particles are different. The siderophores in seawater are marinobactins and amphibactins, whereas the siderophore in particulate matter is ferrioxamine G. Sampling details for particulate matter collection can be found in previous studies⁶⁰.

Extended Data Table 2 | Concentrations of ⁵⁷Fe-siderophores (⁵⁷Fe-S) and ²⁷Al-siderophores (²⁷Al-S) in seawater with depth after five days of incubation

Depth (m)	Peak A (pM)		Peak B (pM)		Peak C (pM)		Peak D (pM)	
	⁵⁷ Fe-S	²⁷ Al-S						
75	45.4	0	41.5	0	52.8	0	20.3	0
100	33.1	0.3	27.1	0.7	34.8	0.9	13.0	0.2
150	38.2	0	37.9	0	57.6	0	21.7	0
200	1.9	0.6	3.0	3.8	0.8	1.8	2.3	1.4
250	6.9	2.0	6.4	4.3	10.6	3.9	4.5	0.6
300	0.6	1.4	0.2	2.6	0.8	1.8	0.3	0.7
350	0.7	2.0	0.5	4.3	0.8	3.4	0.3	0.5
400	0.5	1.3	0.4	4.7	0.6	2.6	0.2	0.8
450	57.2	0	54.4	0	76.6	0	28.0	0
Control (200m)	61.4	0.2	53.8	0.4	94.3	0.6	40.0	0
Control (400m)	58.8	0.1	54.2	0.4	88.3	0.4	37.8	0

Separation and peak identifications are given in Fig. 4. In the euphotic zone to 150 m, the major loss of siderophores is from oxidation as labile carbon and nitrogen. There is little production of ²⁷Al-siderophores. In the mesopelagic (200–400 m), most ⁵⁷Fe-labelled siderophore is used for iron acquisition, and only small amounts of labelled siderophores were recovered at the end of the incubation. Production of ²⁷Al-siderorphores from metal-free siderophores is high. Below 400 m, siderophore concentrations after incubation are similar to values measured in the controls, indicating little uptake for iron acquisition.

Extended Data Table 3 | Total siderophore concentrations for peaks A-D (Fig. 4) after five days of incubation

	Peak A (pM)	Peak B (pM)	Peak C (pM)	Peak D (pM)
75 m	42.1	50.5	49.1	15.8
150 m	52.3	67.6	71.7	22.3
200 m	35.6	40.8	57.6	16.3
400 m	39.7	46.5	55.0	15.9
450 m	64.3	82.2	92.3	29.3
Control	60.1	54.0	91.3	38.9

⁵⁷Total siderophores are the sums of metal-free and ⁵⁷Fe-siderophores for each peak. Approximately 70% of the siderophores were recovered in the euphotic zone and mesopelagic; however, siderophores in the mesopelagic were largely metal-free, while euphotic zone siderophores were bound to ⁵⁷Fe.